Seasonal variation of evapotranspiration and its effect on the surface energy budget closure at a tropical forest over north-east India

Pramit Kumar Deb Burman[1,2,*], Dipankar Sarma[3], Ross Morrison[4], Anandakumar Karipot[2] and Supriyo Chakraborty[1]

[1]*Centre for Climate Change Research, Indian Institute of Tropical Meteorology, Pune 411 008, India.*
[2]*Department of Atmospheric and Space Sciences, Savitribai Phule Pune University, Pune 411 007, India.*
[3]*Department of Environmental Sciences, Tezpur University, Tezpur 784 028, India.*
[4]*Land Surface Science, Hydro-Climate Risks, NERC Centre for Ecology and Hydrology, Wallingford, Oxfordshire OX10 8BB, UK.*
Corresponding author. e-mail: pramit.cat@tropmet.res.in

This study uses 1 yr of eddy covariance (EC) flux observations to investigate seasonal variations in evapotranspiration (ET) and surface energy budget (SEB) closure at a tropical semi-deciduous forest located in north-east India. The annual cycle is divided into four seasons, namely, pre-monsoon, monsoon, post-monsoon and winter. The highest energy balance closure (76%) is observed during pre-monsoon, whereas the lowest level of closure (62%) is observed during winter. Intermediate closure of 68% and 72% is observed during the monsoon and post-monsoon seasons, respectively. Maximum latent heat flux during winter (150 W m^{-2}) is half of the maximum latent heat (300 W m^{-2}) flux during the monsoon. ET is a controlling factor of SEB closure, with the highest rates of closure corresponding to the periods of the highest ET. The Bowen ratio ranges from 0.93 in winter to 0.27 during the monsoon. This is the first time the role of ET in the seasonal variation of SEB closure has been reported for any ecosystem in north-east India using EC measurements.

Keywords. Eddy covariance; Indian summer monsoon; MetFlux India; surface energy budget; tropical forest; India.

1. Introduction

India is one of the most populous countries of the world and has been registering a fast and steady economic growth. As a predominantly agrarian economy, food production and economic activity depend strongly on the Indian summer monsoon (Gadgil and Gadgil 2006). Apart from ecosystem productivity, which is measured as the amount of carbon sequestered by ecosystems (Randerson *et al.* 2002), the dynamics of the monsoon also affects the hydrological cycle of the country. The Indian summer monsoon remains one of the most intriguing but least understood planetary-scale events, despite being subjected to active research over several decades (Goswami and Ajayamohan 2001; Wang 2006).

Evapotranspiration (ET; mm time period^{-1}) is a combined measure of evaporation and transpiration (Wang and Dickinson 2012) which is the latent

heat flux (LE; W m^{-2}) when expressed in energy units. Generally, ET is considered to have three components, namely, water transpired by plants, and evaporation from soil and canopy-intercepted rainfall (Dirmeyer *et al.* 2006). Transpiration is a plant physiological process controlled by multiple physical and meteorological parameters such as precipitation (Giambelluca *et al.* 2009), soil water availability (Fisher *et al.* 2008) and radiation (Si *et al.* 2007). Forests in tropical regions are typically not water stressed due to high annual rainfall (Pejam *et al.* 2006). Moreover, unlike arid and semi-arid regions, plant species have root systems that allow access to water in deeper soil layers (Scott *et al.* 2004; Yaseef *et al.* 2010). Hence, precipitation and/or soil moisture represent less important controls than available energy on ET in such regions.

Many studies have partitioned ET into transpiration and evaporative components using different methods, such as stable isotope analysis (Rothfuss *et al.* 2010), sap flow techniques (Shuttleworth 2007), as well as empirical and process models (Kool *et al.* 2014). Several researchers have also studied relationships between the transpiration component and incoming photosynthetic photon flux density (PPFD; μmol photons m^{-2} s^{-1}) (Wilson and Baldocchi 2000; Bovard *et al.* 2005).

ET represents one of the most important components of the hydrological cycle. Several recent studies have reported that ET from the Indian landmass is experiencing a decreasing trend in response to anthropogenic climate change (Jhajharia *et al.* 2009; Mukhopadhyay *et al.* 2017). At a smaller scale, ET has a strong dependence on land cover. Croplands and forest ecosystems, e.g., have different ET dynamics due to contrasting biological responses to environmental conditions and management, such as soil water availability and irrigation scheduling, respectively (Wang and Dickinson 2012). Modelling and observational studies show that ecosystems in the humid tropics have larger ET compared to ecosystems in other climatic regions (Fisher *et al.* 2009; Jung *et al.* 2011). Global ET studies (e.g., Jung *et al.* 2011) have also highlighted the strong ET flux from Indian ecosystems to the atmosphere, with dense areas of pristine forests in north-east India showing particularly high rates. To date, such analyses in India have been based on coarse meteorological data and/or satellite-derived products as higher temporal frequency, as surface-based observations have not been available.

ET is an integral part of the surface energy budget (SEB). In India, there have been multiple field campaigns to study boundary layer evolution and surface fluxes and their interactions with the Indian summer monsoon (Bhat and Narasimha 2007). These experiments were primarily aimed at improving numerical weather forecasting models by providing improved momentum and sensible heat flux parameterisations. However, these campaigns were conducted over short time scales (MONTBLEX) (Sikka and Narasimha 1995) and/or did not consider all components of the SEB (LASPEX) (Vernekar *et al.* 2003). Based on a 5-month long tower-based observation around the monsoon period in Bangalore, Bhat and Arunchandra (2009) reported that the longwave radiation and LE are the largest sources of uncertainty in the SEB closure. From a study conducted in Bangalore during the monsoons of 2009 and 2010, as part of the PROWNAM campaign, Reddy and Rao (2018) showed that the shortwave radiation and H vary by 407 and 126 W m^{-2} between the convective and non-convective conditions. LE was found to be higher than H throughout a 1-year long measurement period during 1996–1997 at Lucknow by Ramana *et al.* (2004).

More recently, the SEB has been explored at a range of Indian ecosystems using different methodologies, such as, flux-gradient relationships, similarity theory or eddy covariance (EC) measurements. It is generally accepted that the EC is currently the most defensible approach to quantify surface-atmosphere energy fluxes (Baldocchi 2014); however, a key issue is a near-ubiquitous imbalance between EC-based observations of turbulent energy fluxes when compared with independent observations of the available energy (Leuning *et al.* 2012).

Several EC flux towers have now been established over different ecosystems across India (Jha *et al.* 2013; Rodda *et al.* 2016). Whereas diurnal, seasonal and inter-seasonal variations of water and carbon dioxide fluxes have been reported for several ecosystems, the dynamics of the surface energy balance have not been studied in detail. In other regions, EC analyses often divide the annual cycle into two contrasting periods, such as wet and dry (Eamus *et al.* 2001) or growing and post-harvest (Scott *et al.* 2004). For India, four distinct seasons have been classified, which are closely associated with the Indian summer monsoon (Wang 2006). To the best of our knowledge, no study has yet quantified the variation of SEB closure according to these four seasons. Moreover, the influence

of ET measured from high-frequency, in situ, EC measurements on SEB remains largely unexplored. Although the surface energy imbalance is nearly always observed in the EC-based studies, none of the studies has explored this in detail.

MetFlux India is a project initiated by the Indian Institute of Tropical Meteorology (IITM) in Pune and funded by the Ministry of Earth Sciences (MoES), Government of India. It is inspired by Fluxnet, the global network of EC flux towers (Baldocchi *et al.* 2001). Under MetFlux India, three new micrometeorological flux towers have been set up to monitor fluxes at forest ecosystems, including the semi-deciduous forest in north-east India, the evergreen coniferous forest in the eastern Himalaya (Chatterjee *et al.* 2018) and the mangrove forest in the Bay of Bengal (Gnanamoorthy *et al.* 2019). Multi-year observations from MetFlux India stations will deliver long-term and continuous records of biosphere–atmosphere carbon, water and energy fluxes.

The objectives of this study were: (i) to quantify seasonals variations of SEB at a tropical semi-deciduous forest using the EC technique; (ii) to enhance the surface energy imbalance by parameterising the soil heat flux and (iii) to analyse the role of ET as a control on seasonal variations in the level of SEB closure.

2. Material and methods

2.1 *Site*

A 50-m tall micrometeorological tower ($26°34'$ N, $93°6'$ E; figure 1) was established in Kaziranga National Park (KNP) in 2014 as part of a collaboration between IITM and Tezpur University. The flux observation site is a moist semi-deciduous forest with an average canopy height of 20 m. The climate is humid sub-tropical (CWa type) according to the Köppen classification scheme (Kottek *et al.* 2006). In this study, a 1-year record of fluxes and supporting micrometeorological observations from 2016 is analysed and reported. Full details of the site can be found in Deb Burman *et al.* (2017).

2.2 *Instrumentation*

The EC system was installed at a height of 37 m above the soil surface. The EC instrumentation consists of a WindMaster Pro 3D sonic anemometer–thermometer (Gill Instruments, Lymington, UK), measuring zonal (u in m s^{-1}),

Figure 1. Map of India showing the location (tower symbol) of the micrometeorological flux tower at KNP in north-east India.

meridional (v in m s^{-1}) and vertical (w in m s^{-1}) wind components at a temporal resolution of 10 Hz, combined with an LI-7200 enclosed path CO_2/H_2O infrared gas analyser (IRGA, Li-COR Biosciences, Lincoln, USA). Four WXT520 multi-component weather sensors (Vaisala Oyj., Vantaa, Finland) were installed at heights of 4, 7, 20 and 37 m, each providing measurements of ambient air temperature (T_a in K), air pressure (P in hPa), rainfall (daily total precipitation (precip) in mm) and relative humidity (RH in %) at 1-min intervals. Soil temperature (T_s in K) and moisture content (SWC in m^3 m^{-3}) were recorded every 1 min by 5TE water content, electrical conductivity and temperature sensors installed at five different depths (surface, 0.05, 0.15, 0.25 and 0.40 m). Two HPF01SC-20 soil heat flux plates (HukseFlux, Manorville, USA) were installed at a depth of 0.05 m for measuring the ground heat flux (G in W m^{-2}) every minute. Net radiation (R_n in W m^{-2}) and its four components, namely, incoming shortwave radiation (R_{SW}(in) in W m^{-2}), incoming longwave radiation (R_{LW}(in) in W m^{-2}), outgoing shortwave radiation (R_{SW}(out) in W m^{-2}) and outgoing longwave radiation (R_{SW}(out) in W m^{-2}) were measured every

Table 1. *Instruments and variables used. Depths within the soil are marked negative.*

Instrument	Model and manufacturer	Altitude of measurement (m)	Variable (unit)	Temporal resolution (s)	Accuracy
Multi-component weather sensor	WXT520, Vaisala Oyj., Vantaa, Finland	4, 7, 20, 37	T_a (K), P (hPa), precip (mm)	60	±0.3 K for T_a, ±0.5 hPa for P and ≤ 5% for precip
3D Sonic anemometer-thermometer	WindMaster Pro, Gill Instruments, Lymington, UK	37	u (m s^{-1}), v (m s^{-1}), w (m s^{-1})	0.1	<1.5% RMS (root mean square)
CO_2 and H_2O infrared gas analysers	IRGA Model: LI-7200 enclosed path CO_2/H_2O analyser, Li-COR Biosciences, Lincoln, USA	37	c (μmol m^{-3}), q (g kg^{-1})	0.1	Within 1% and 2% of readings for CO_2 and H_2O measurements, respectively
Four-component net radiometer	NR01, Hukseflux, Manorville, NY, USA	19	R_{SW}(in) (W m^{-2}), R_{LW}(in) (W m^{-2}), R_{SW}(out) (W m^{-2}), R_{LW}(out) (W m^{-2}), R_n (W m^{-2})	60	<15 W m^{-2}
Quantum sensor	SQ-110, Apogee Instruments, Inc., Logan, Utah, USA	19	PPFD (μmol m^{-3})	60	±5%
Soil heat flux plate	HFP01SC-20, Campbell Scientific, Logan, Utah, USA	−0.05	G (W m^{-2})	60	±3%

1 min by a NR01 4-component net radiometer (HukseFlux, Manorville, USA). PPFD in μmol m^{-2} s^{-1} was measured every 1 min by a SQ-110 Sun calibrated quantum sensor (Apogee Instruments Inc., Logan, Utah, USA). These two instruments were installed at a height of 19 m on the tower. Additionally, half-hourly averaged records of all variables were also created and logged using two CR3000 data loggers (Campbell Scientific, Logan, Utah, USA). Details of the above-mentioned instrumentation and variables are summarised in table 1.

2.3 Data handling

2.3.1 Flux calculation from EC data

Sensible (H in W m^{-2}) and latent (LE in W m^{-2}) heat fluxes are computed from the raw EC data following Reynolds averaging (Aubinet *et al.* 2012) using EddyPro version 6.2.0 (https://www.licor.com). High-frequency measurements by the EC system are often contaminated by various types of errors that require correction (Burba 2013) such as obtrusive angle of flow, random spikes, instrumental offset, non-ideal geometry, etc. These errors originate for different reasons ranging from instrumental limitations to faulty experimental set-up. Hence, before computing fluxes, raw EC data are subjected to rigorous quality control measures, including angle of attack correction (Nakai *et al.* 2006), despiking (Mauder *et al.* 2013), block averaged detrending (Kaimal and Finnigan 1994) and dual-axis coordinate rotation (Kaimal and Finnigan 1994). Due to the physical separation between the sonic anemometer and an infrared gas analyser (IRGA), a time lag is introduced between the measured wind components and gaseous mixing ratios (c and q) which is compensated by applying a time lag correction (Burba 2013). High- (Moncrieff *et al.* 2004) and low-pass corrections (Moncrieff *et al.* 1997) are applied to compensate for the loss of flux towards the low and high-frequency ranges of the cross-spectrum, respectively. Such losses can

Table 2. *Biometeorological variables required for quality control and gap filling of the flux data. Depths within the soil are marked negative.*

Variable (unit)	Instrument	Model and manufacturer	Altitude/depth of measurement (m)	Temporal resolution (m)	Accuracy
T_a (K)	Multi-component weather sensor	WXT520, Vaisala Oyj., Vantaa, Finland	4, 7, 20, 37	1, 30	±0.3 K
P (hPa)	Multi-component weather sensor	WXT520, Vaisala Oyj., Vantaa, Finland	4, 7, 20, 37	1, 30	±0.5 hPa
RH (%)	Multi-component weather sensor	WXT520, Vaisala Oyj., Vantaa, Finland	4, 7, 20, 37	1, 30	±3%
T_s (K)	Water content, electrical conductivity and temperature sensor	5TE, Decagon Devices Inc., Pullman, Washington, USA	surface, −0.05, −0.15, −0.25, −0.40	1, 30	±1 K
SWC ($m^3 m^{-3}$)	Water content, electrical conductivity and temperature sensor	5TE, Decagon Devices Inc., Pullman, Washington, USA	surface, −0.05, −0.15, −0.25, −0.40	1, 30	±15%

arise out of inefficient filtering and/or time averaging (Burba 2013). The WPL correction (Webb *et al.* 1980) was applied while calculating fluxes from the gaseous mixing ratios to remove the effect of humidity and temperature.

2.3.2 *Post-processing and quality control of flux data*

Half-hourly averaged values of T_a, T_s, RH, SWC, R_{SW}(in), R_{LW}(in), R_{SW}(out), R_{LW}(out), R_n, PPFD and G are aggregated into a biometeorological file to be used as an additional input to EddyPro. These variables are measured with a lower time resolution than EC. The full output of EddyPro contains these biometeorological variables, averaged and time-synchronised with calculated fluxes. Random uncertainties arising out of the flux-sampling error are computed following Finkelstein and Sims (2001). A daily quality control file is also generated along with the fluxes, containing statistical parameters and flags for stationarity and well-developed turbulence tests for the calculated fluxes (Foken *et al.* 2004). Outliers in H and LE data were detected and removed by the median absolute deviation (MAD) (Sachs 1997)

technique and removed following Papale *et al.* (2006) (table 2).

2.3.3 *Gap-filling of flux and meteorological data*

Long-term records of meteorological and flux variables inevitably experience data gaps related to sensor or system malfunctions, unfavourable measurement conditions or insufficient power, as well as data-filtering during QC (Moffat *et al.* 2007). In this study, flux data gaps are filled using the REddyProc package (Wutzler *et al.* 2018) for the R Language (R Core Team). It offers various mechanisms to be applied for filling the gaps. In the present work, the marginal distribution sampling (MDS) approach (Reichstein *et al.* 2005) is used to fill gaps in H, LE, R_n, R_{SW}(in), G and PPFD.

2.3.4 *Parameterisation of soil heat flux*

Soil heat flux (G) is an important component of the SEB. It is directly measured by soil heat flux sensors installed within the top soil layer. The observation of G suffers from frequent data loss due to water logging, power failure, sensor damage and malfunctioning (Sauer *et al.* 2007) and the underestimations in G result in the non-closure of

the SEB (Heusinkveld *et al.* 2004). Attempts have been made by several researchers to address this potential problem by the indirect estimates of G. Daughtry *et al.* (1990) and Kustas and Daughtry (1990) compared estimates of G based on remote sensing against a set of distributed soil heat flux plates. It was seen to reduce the error in SEB significantly. Other such methods include calculating G from the soil temperature and moisture (Yang and Wang 2008), from relationships with vegetation indices (Kustas *et al.* 1993) and correcting G in conjunction with the Bowen ratio method (de Silans *et al.* 1997), etc.

The forest floor at KNP remains waterlogged during most of the monsoon and post-monsoon seasons due to heavy and frequent rainfall. Due to the presence of dark cumulus clouds and dense vegetation canopy, the least amount of sunlight penetrates through the forest. Such conditions resulted in insufficient charging of the solar cells, causing power shortage. As direct electricity connection could not be provided within the forest, all instruments and sensors were powered by solar cells. Hence, during most of the monsoon and post-monsoon seasons, sensors remained inactive and frequent long data gaps were observed in G. For filling up the longer gaps in G, a simplistic parameterisation scheme was devised between R_n and G by Purdy *et al.* (2016), indicating that such schemes are widely used globally and are better-suited to capture the high-frequency variations compared to the other schemes.

The boundary between daytime and night-time conditions was defined using $R_{SW}(in) \geq 20$ W m^{-2} and $R_{SW}(in) < 20$ W m^{-2}, respectively. This is an objective criterion based on Reichstein *et al.* (2005). Following this, available half-hourly data are divided into daytime and night-time. For both of these times, scatter plots are made between R_n and G. Assuming a linear relationship between R_n and G (Idso *et al.* 1975; Norman *et al.* 2000), two different straight lines are fit to these scatter plots. These straight-line fits are further separately used for interpolating G using R_n during daytime and night-time. Finally, daytime and night-time values are merged together to create a continuous half-hourly record of G.

2.3.5 *Calculation of vapour pressure deficit (VPD)*

VPD is defined as the difference between saturation water vapour pressure and measured water vapour pressure at a given air temperature (Monteith 1965). It is the measure of the moisture-holding capacity of the atmosphere at that particular temperature (Wang and Dickinson 2012). We have calculated VPD from T_a and RH using REddyProc. Existing gaps in T_a and RH propagate in VPD which are filled by the MDS algorithm using REddyProc.

2.3.6 *Seasonal variation*

To analyse seasonal patterns, observations obtained during 2016 were divided into four seasons, namely, monsoon, post-monsoon, winter and pre-monsoon. The Indian landmass gets immensely heated up during summer due to the enhanced amount of incoming solar radiation. This results in a distinct land ocean temperature gradient (Xavier *et al.* 2007). As a result, moisture-laden south-westerly winds flow into the peninsular India from the Arabian Sea bringing in an enhanced amount of rainfall. According to Wang and Ho (2002), the total annual rainfall is concentrated in the months of summer (June, July, August and September, abbreviated as JJAS), often identified as the monsoon. Monsoon withdrawal takes place in the month of October (Wang 2006).

The months after the withdrawal of the Indian summer monsoon are characterised by a receding amount of rainfall and decreasing temperatures (Jain and Kumar 2012). Hence the months of October and November, abbreviated as ON, are defined as the post-monsoon months (Hingane *et al.* 1985; Singh *et al.* 2000). Winter is defined as the months of December, January and February, abbreviated as DJF (Hingane *et al.* 1985). During this period, the land–ocean temperature gradient is reversed due to the cooling of the land caused by a decreased amount of incoming solar radiation. This results in the reversal of the near-surface wind over the Indian landmass (Wang 2006). Annual minimum air temperature is observed during these months (Jain and Kumar 2012). This is also the driest period of the year, recording a minimum amount of rainfall (Parthasarathy *et al.* 1994). Air temperature starts rising in the month of March and continues the increasing trend until the end of May, causing an intense heating of the Indian landmass in the process. Pre-monsoon heating plays a crucial role in reversing the land–ocean temperature gradient and the total amount of rainfall all over India during the monsoon (Parthasarathy *et al.* 1990). The onset of monsoon takes place in the first week of June. Hence, the months of March,

April and May, abbreviated as MAM is defined as pre-monsoon (Hingane *et al.* 1985; Jain and Kumar 2012).

2.3.7 *SEB and Bowen ratio*

The SEB is the manifestation of the conservation of energy at the Earth's surface. Net radiation (R_n) reaching the Earth's surface is calculated from the incoming and outgoing radiation components, using

$$R_n = R_{SW}(in) + R_{LW}(in)$$
$$- R_{SW}(out) - R_{LW}(out), \qquad (1)$$

where all variables are defined above. R_n is further partitioned into sensible (H), latent (LE) and soil (G) heat fluxes, as

$$R_n = H + LE + G. \qquad (2)$$

Complete energy balance closure (e.g., energy conservation) should result in a linear relationship with a slope of unity for ($R_n - G$) versus ($H + LE$) (Stull 2012). However, full closure is rarely met using EC measurements due to unaccounted energy fluxes from advection, heat storage in air, soils and biomass (Leuning *et al.* 2012; Burba 2013) and larger-scale atmospheric motions (Fisher *et al.* 2008). This energy imbalance can translate either into an overestimation of H and LE or an underestimation of R_n (Aubinet *et al.* 2012), and either of these erroneous estimates is reflected by the y-intercept of the SEB scatter plot. In this study, energy balance closure is reconstructed and analysed for each of the four seasons and the y-intercept of the SEB scatter plot is referred to as the residual energy in this paper.

The Bowen ratio (β) is defined as the ratio of sensibility to LEs (Tanner 1960), as

$$\beta = H/LE. \qquad (3)$$

The Bowen ratio has been widely used for estimating LE from observations of H (Dugas *et al.* 1991; Shi *et al.* 2008) following the assumption of full SEB closure (Malek and Bingham 1993; Twine *et al.* 2000; Gu *et al.* 2005; Tsai *et al.* 2010; Cho *et al.* 2012). Generally, the midday value of β is preferred for the analyses (Jarvis *et al.* 1997) as maximum values of H and LE are observed around midday. For the present work, table 3 lists the seasonal values of SEB closure, residual energy and β.

3. Results

Annual meteorology at KNP for 2016 is shown in figure 2. Half-hourly records of T_a, P and precip are available at four different heights (table 3). For each of these variables, the mean of the four records is calculated. Furthermore, daily averaged values of T_a and P have been calculated from their average half-hourly records. Daily total values of precip are calculated by summing up the average half-hourly record over the duration of each day. Figure 2(a–c) shows daily values of T_a, P and precip respectively, calculated this way.

Prominent seasonal variations are seen in each of the three variables mentioned above. Annual minimum and maximum T_a are 285 and 305 K which are recorded in winter and monsoon, respectively. T_a starts increasing towards the end of winter and continues rising during pre-monsoon. T_a attains the peak value during the monsoon and starts decreasing by the end of the monsoon. A sharp decline is observed in T_a during post-monsoon. Unlike during pre-monsoon and post-monsoon, T_a remains stable during the monsoon and does not change rapidly with time. Finally, T_a drops down to its minimum value in winter.

P showed a rapid decline and growth during pre-monsoon and post-monsoon, respectively. Maximum P (figure 2) was observed during winter (1010 hPa). P decreased continuously in the pre-monsoon season and attained a minimum value of 990 hPa during the monsoon. P increased during post-monsoon. The annual pattern of P shows contrasting trends to T_a. Similar to T_a, P remained stable with low variability during the monsoon.

Table 3. *SEB closure, residual energy and β during different seasons.*

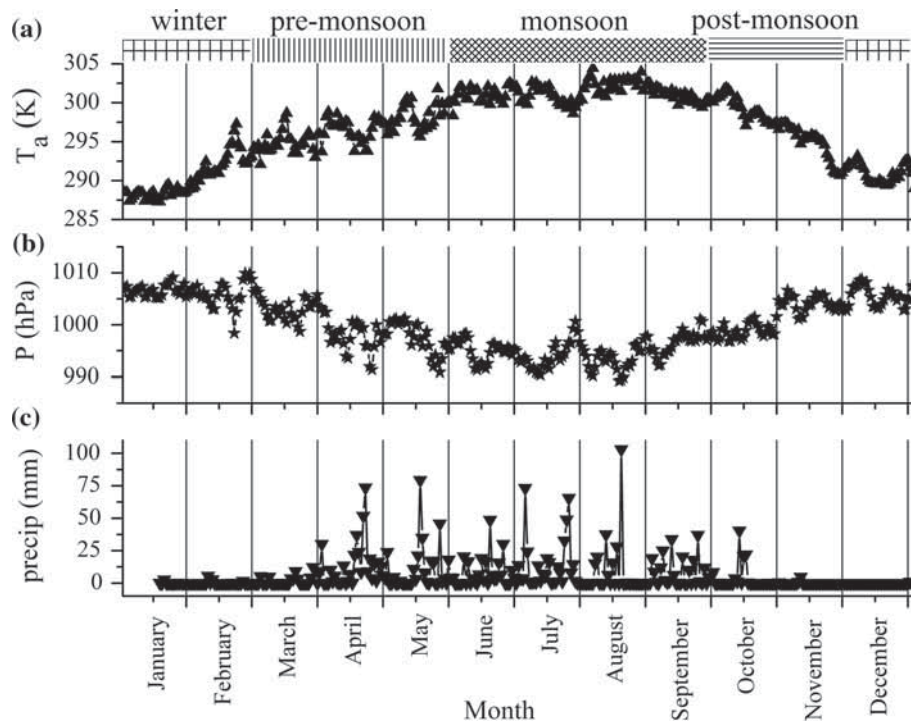| Season (months)	SEB closure (%)	Residual energy flu (W m^{-2})	B (at 12.0 hr)
Pre-monsoon (MAM)	76	8.53	0.33
Monsoon (JJAS)	68	5.11	0.27
Post-monsoon (ON)	72	15.36	0.37
Winter (DJF)	62	15.55	0.93

Figure 2. Annual variations of (**a**) daily averaged air temperature (T_a), (**b**) daily averaged air pressure (P) and (**c**) daily total precipitation (precip) at KNP for 2016. Different seasons are indicated at the top of the figure.

Winter is the driest season at KNP with a negligible amount of rainfall observed during this season. KNP started receiving rainfall in April, with daily values of around 75 mm recorded during April and May. The monsoon season experiences the highest amounts of rainfall, with values of 100 mm day^{-1} observed during this period. Daily rainfall totals start decreasing towards the end of monsoon, with fewer more isolated rainfall events observed during the post-monsoon season.

The scatter plot of half-hourly records of R_n and LE for the entire measurement period is presented in figure 3. As expected, LE increases with increasing R_n. As a first approach towards evaluating the SEB, the long data gaps in G are ignored. This way, the linear fit between the available energy $(R_n - G)$ and the sum of the turbulent energy fluxes $(LE + H)$ (figure 4) is statistically significant, and shows that SEB closure is 69% ($y = 0.69x + 9.89$, adjusted $R^2 = 0.84$, $p < 0.05$), with an energy imbalance of 31%.

In order to improve the SEB closure, G is parameterised using the method described in section 2.2. A linear relationship is assumed between G and R_n throughout the day, with different slopes and intercepts for daytime and night-time (figure 5). The differences between day and night reflect lower turbulent energy exchanges relative to
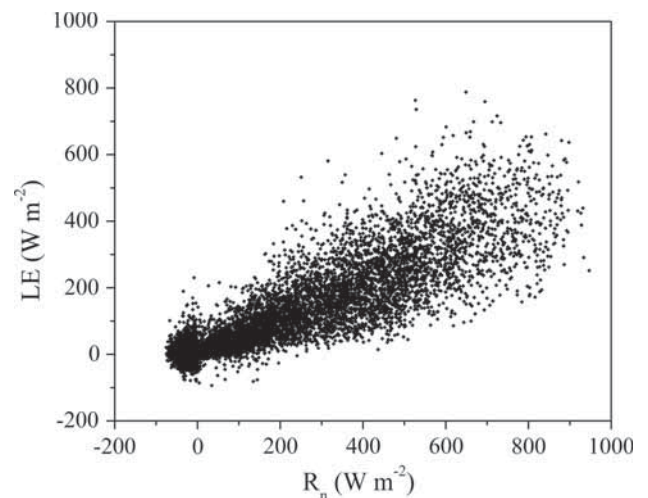

Figure 3. Scatter plot between half-hourly values of net radiation (R_n) and LE observed at KNP during 2016.

daytime conditions. For daytime conditions, a linear fit indicated that G increases by 2.5% of R_n ($y = 0.025x + 0.22$, $p < 0.05$). For nocturnal conditions, G decreases by 3.2% of R_n ($y = -0.032x - 5.24$, $p < 0.05$).

Remaining daytime and night-time gaps in G are filled using the relationships described above. This gap-filled record of G is referred to as the parameterised G, and is used to represent soil heat fluxes
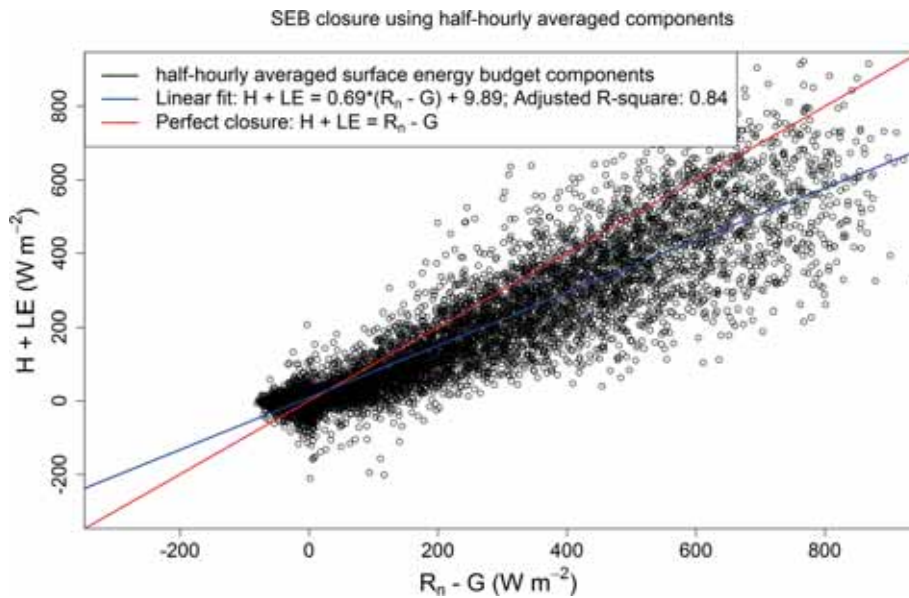
Figure 4. SEB closure at KNP for 2016 using half-hourly averaged values of net radiation (R_n), sensible heat flux (H), LE and soil heat flux (G).

in the remainder of the paper, unless indicated otherwise. The linear fit between the available energy (calculated using parameterised G) and the turbulent energy fluxes ($y = 0.70x + 10.36$, adjusted $R^2 = 0.87$, $p < 0.05$) shows closure increases by 1% compared to the previous fit (figure 6). Daily averaged values of R_n, G, H and LE are calculated from their half-hourly records. The linear fit to the daily values indicated SEB closure of 80% ($y = 0.8x + 0.04$, adjusted $R^2 = 0.87$, $p < 0.05$), improving SEB closure by 10% compared to linear fits based on 30-min observations (figure 7).

Mean diurnal variations of R_n, $R_\mathrm{SW}(\mathrm{in})$, H and LE during pre-monsoon (MAM), monsoon (JJAS), post-monsoon (ON) and winter (DJF) are presented in figure 8. Prominent seasonal variation is observed in R_n. Maximum values of R_n during pre-monsoon, monsoon, post-monsoon and winter are approximately 500, 550, 525 and 400 W m^{-2}, respectively. Negative values of R_n are observed at night. The most negative R_n is observed during winter and the least negative values are observed in the monsoon season. A closer inspection of the diurnal variations reveals that during winter, R_n starts increasing around 6.5 hr, becomes positive around 7.5 hr, reaches maximum around 11.0 hr and starts decreasing thereafter. While decreasing, it becomes zero around 16.0 hr. It reaches a minimum value of -50 W m^{-2} at 17.5 hr. On the other hand, during the monsoon, R_n starts increasing around 5.0 hr, becomes

positive at 6.0 hr, reaches maximum at 12.5 hr and then onwards, starts decreasing. It becomes zero at 18.0 hr while decreasing and reaches a minimum value of -25 W m^{-2} at 19.0 hr. During pre-monsoon, R_n starts increasing around 5.5 hr, becomes positive around 6.5 hr, reaches the maximum around 12.0 hr and starts decreasing onwards. It becomes negative at 17.5 hr and reaches the minimum value of -30 W m^{-2} around 18.5 hr. Finally, during post-monsoon, R_n registers an increasing trend around 5.5 hr, becomes positive around 6.0 hr, reaches maximum around 12.0 hr and then onwards, starts decreasing. While decreasing, it becomes negative at 16.0 hr and records a minimum value around 17.5 hr.

The maximum values of $R_\mathrm{SW}(\mathrm{in})$ during pre-monsoon, monsoon, post-monsoon and winter are 625, 650, 650 and 550 W m^{-2}, respectively (figure 8). $R_\mathrm{SW}(\mathrm{in})$ remains zero during night-time throughout the seasons. During winter, it starts increasing around 6.0 hr, reaches maximum around 12.5 hr and decreases to zero around 18.0 hr. On the other hand, during the monsoon, $R_\mathrm{SW}(\mathrm{in})$ starts increasing around 5.5 hr, reaches maximum around 13.0 hr and decreases to zero around 19.0 hr. During pre-monsoon, $R_\mathrm{SW}(\mathrm{in})$ starts increasing around 5.5 hr, reaches maximum around 12.0 hr and decreases to zero around 19.0 hr. Finally, during post-monsoon, $R_\mathrm{SW}(\mathrm{in})$ starts increasing at 6.0 hr, reaches maximum around 11.0 hr and decreases to zero around 17.5 hr.
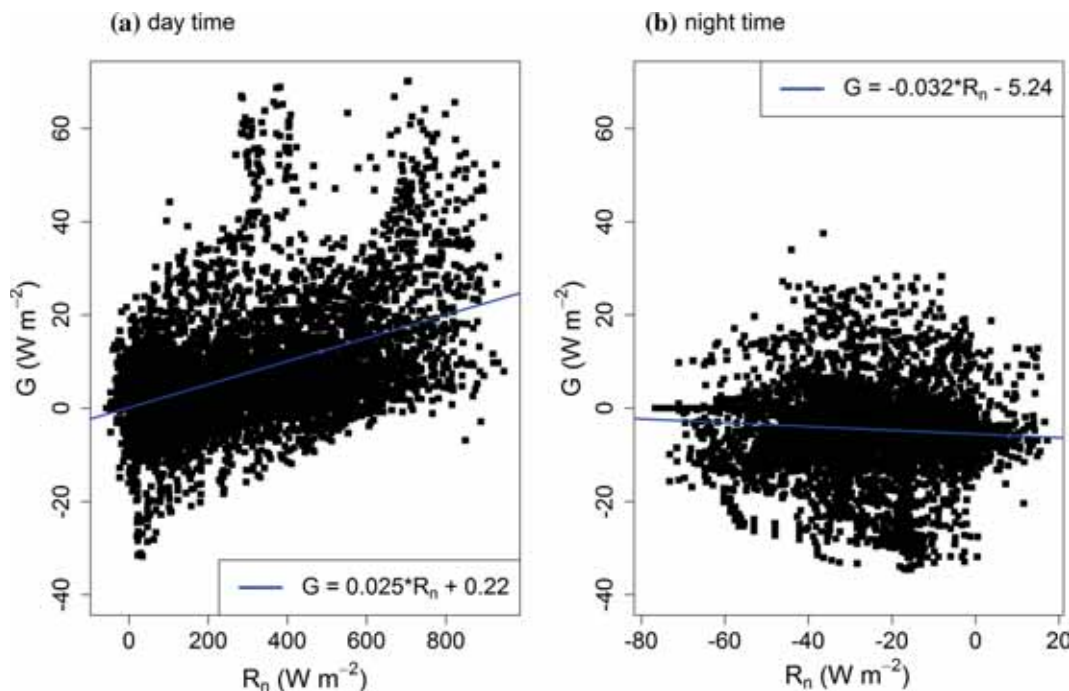
Figure 5. Scatter plots and linear fits between net radiation (R_n) and soil heat flux (G) during (**a**) daytime and (**b**) night-time for KNP in 2016. Daytime is defined using $(R_{SW}(\text{in})) \geq 20$ W m^{-2}. Governing equation for each of the fits is given in the respective figure legends.
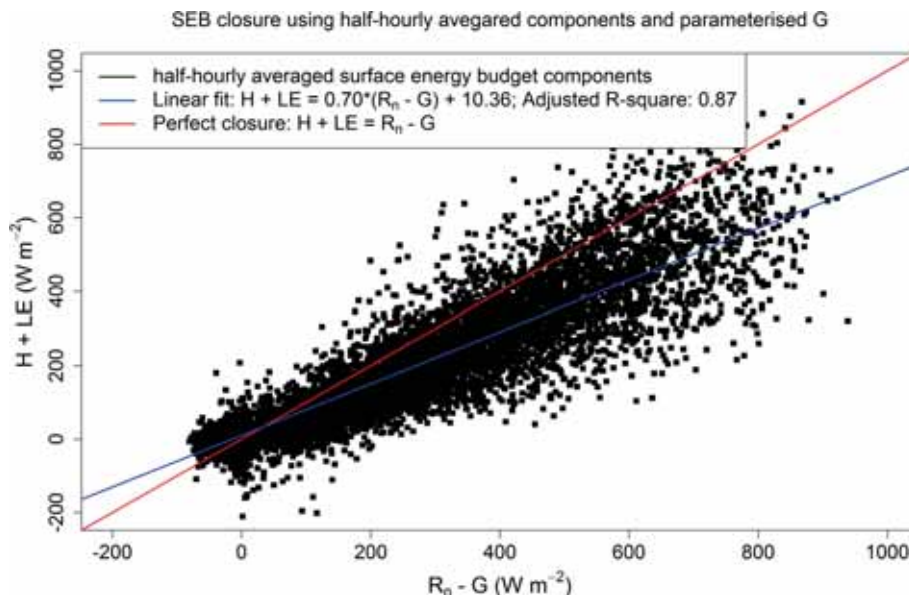

Figure 6. SEB closure at KNP for 2016 using half-hourly averaged values of net radiation (R_n), sensible heat flux (H), LE and soil heat flux (G). G has been parameterised from R_n.

The maximum values of H that are observed during different seasons are: 100 W m^{-2} during pre-monsoon, 85 W m^{-2} during the monsoon, 110 W m^{-2} during post-monsoon and 140 W m^{-2} during winter (figure 8). Throughout the seasons, H is positive during daytime and negative during night-time. During pre-monsoon, the minimum value of H is -20 W m^{-2} which is recorded at night. It increases and becomes positive at 7.5 hr. It reaches the maximum value at 12.0 hr and starts decreasing onwards. While decreasing, it becomes negative at 16.0 hr. During the monsoon, H records a minimum value of -10 W m^{-2} at night. It becomes positive around 6.0 hr. It remains
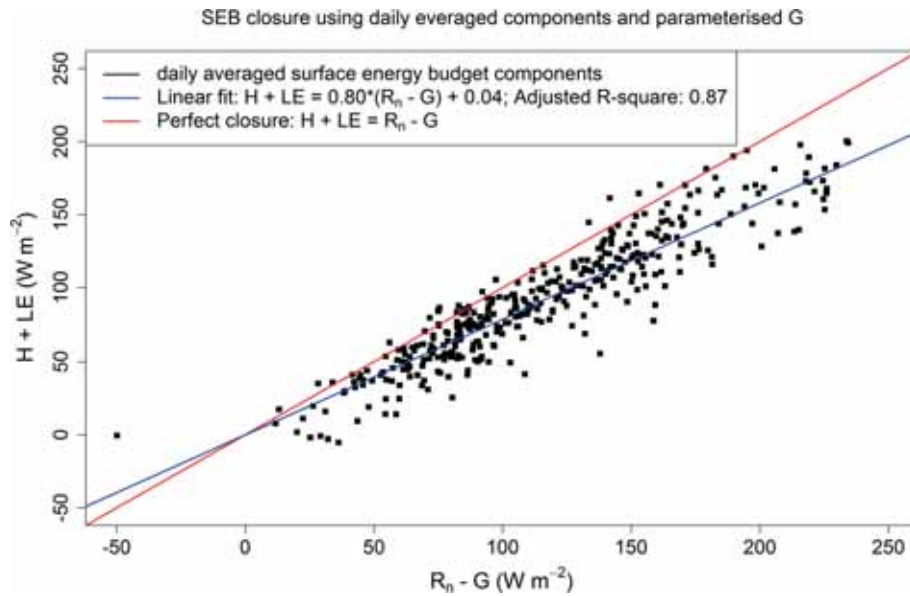
Figure 7. SEB closure at KNP for 2016 using daily averaged values of net radiation (R_n), sensible heat flux (H), LE and soil heat flux (G). G has been parameterised from R_n.
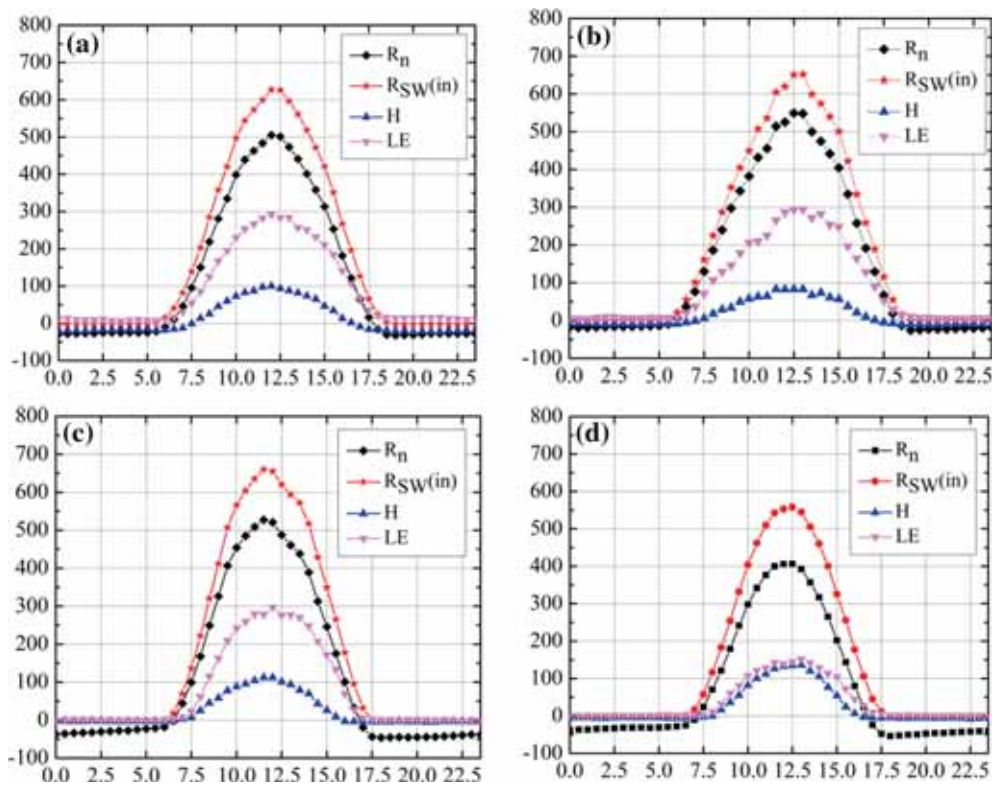

Figure 8. Mean diurnal variations of net radiation (R_n), incoming shortwave radiation ($R_{SW}(in)$), sensible heat flux (H), and LE at KNP during 2016 for (**a**) pre-monsoon, (**b**) monsoon, (**c**) post-monsoon and (**d**) winter. The x-axis and y-axis in all sub-plots show time (hr) (local time) and the different energy fluxes (W m^{-2}).

maximum until 13.0 hr from 11.0 hr. Furthermore, it starts decreasing and becomes negative around 17.0 hr. During post-monsoon, H remains negative but close to zero during night-time. It increases and becomes positive around 6.0 hr. It further increases and becomes maximum around 11.0 hr. It decreases onwards and becomes negative around 16.0 hr. In winter, during night-time, H remains more negative than during the monsoon but less negative than during post-monsoon. It increases
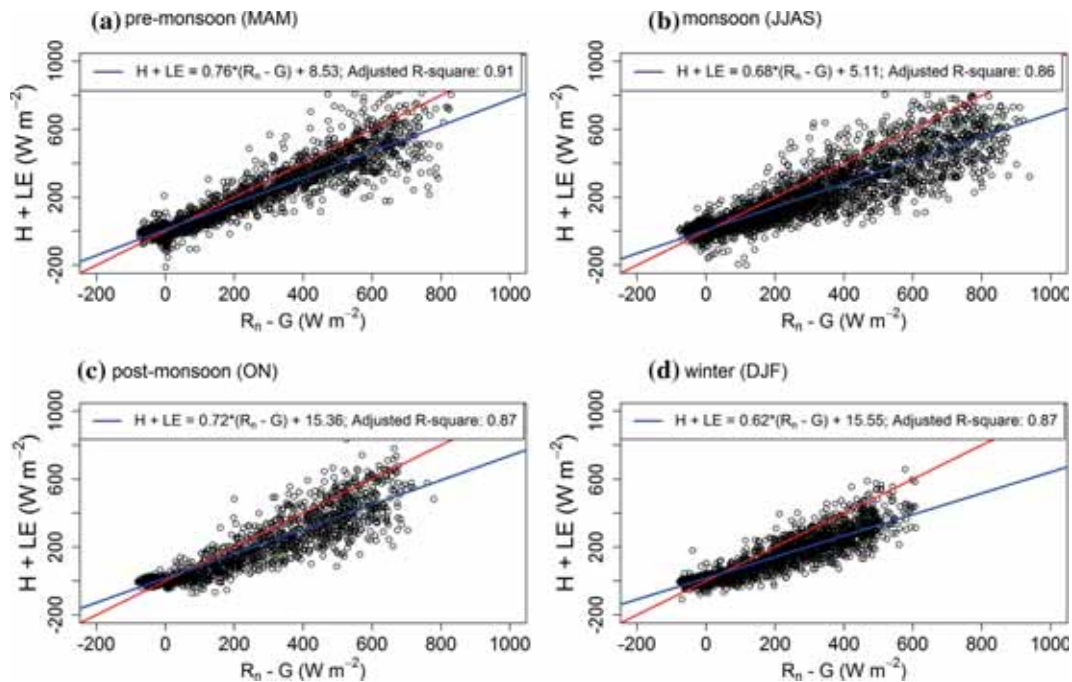
Figure 9. SEB closure at KNP for (**a**) pre-monsoon (MAM), (**b**) monsoon (JJAS), (**c**) post-monsoon (ON) and (**d**) winter (DJF) during 2016 using half-hourly averaged values of net radiation (R_n), sensible heat flux (H), LE and soil heat flux (G). G has been parameterised from R_n. Red continuous lines represent the ideal closure with unit slope. Blue continuous lines represent the linear fits between ($R_n - G$) and ($H + LE$) as obtained from the data using the least-squares method. Governing equation and the adjusted R-squared values for each of the fits are given in the respective figure legends.

and becomes positive around 9.0 hr. The maximum value of H is reached at 13.0 hr. After that, H starts decreasing and becomes negative at 16.0 hr.

A maximum value of 300 W m^{-2} is observed for LE during pre-monsoon, monsoon and post-monsoon (figure 8). During winter, maximum LE is reduced to 150 W m^{-2}. LE is close to zero during the nocturnal periods for the post-monsoon and winter seasons. LE remains non-zero and positive at night during the monsoon and post-monsoon periods. During pre-monsoon, LE starts rising at 6.0 hr, reaches a maximum at 12.0 hr and starts decreasing thereafter. It reaches a minimum value of 25 W m^{-2} at 19.0 hr which is maintained for the rest of the night. In quite a similar fashion, LE starts increasing around 6.0 hr during the monsoon. However, it reaches the maximum value around 12.5 hr. Furthermore, it records a decreasing pattern and reaches the minimum value of 25 W m^{-2} around 19.0 hr. This minimum value is maintained throughout the night. For a long time, it was understood that transpiration stops at night due to the stomatal closure in the absence of solar radiation (Dawson *et al.* 2007; Wang and Dickinson 2012). However, several studies confirmed that night-time respiration forms a significant component of the total transpiration.

Night-time transpiration is stronger in plants and crops that are grown in a water unstressed environment (Caird *et al.* 2007; Novick *et al.* 2009). During post-monsoon, LE starts increasing around 9.0 hr, reaches maximum around 12.0 hr and decreases onwards. It drops to the minimum value of 15 W m^{-2} at 18.0 hr which is maintained throughout the rest of the night. During winter, LE starts increasing at 7.5 hr and reaches maximum at 13.0 hr before dropping to a minimum of zero at 18.0 hr.

Half-hourly components of SEB are estimated separately for different seasons. SEB is computed for each of the seasons using equation (2). Scatter plots between ($R_n - G$) and ($H + LE$) for pre-monsoon, monsoon, post-monsoon and winter have been shown in figure 9. Panels (a–d) of figure 9 correspond to pre-monsoon, monsoon, post-monsoon and winter, respectively. For each of the seasons, linear relationships are fit by least-squares method in R to the scatter plots which are also shown in these figures. Equations governing these fits and the corresponding adjusted R-square values are provided in figure 9.

High R-square values (figure 9) show that all fits are representative of the interrelations among the SEB components. The highest (76%) and the
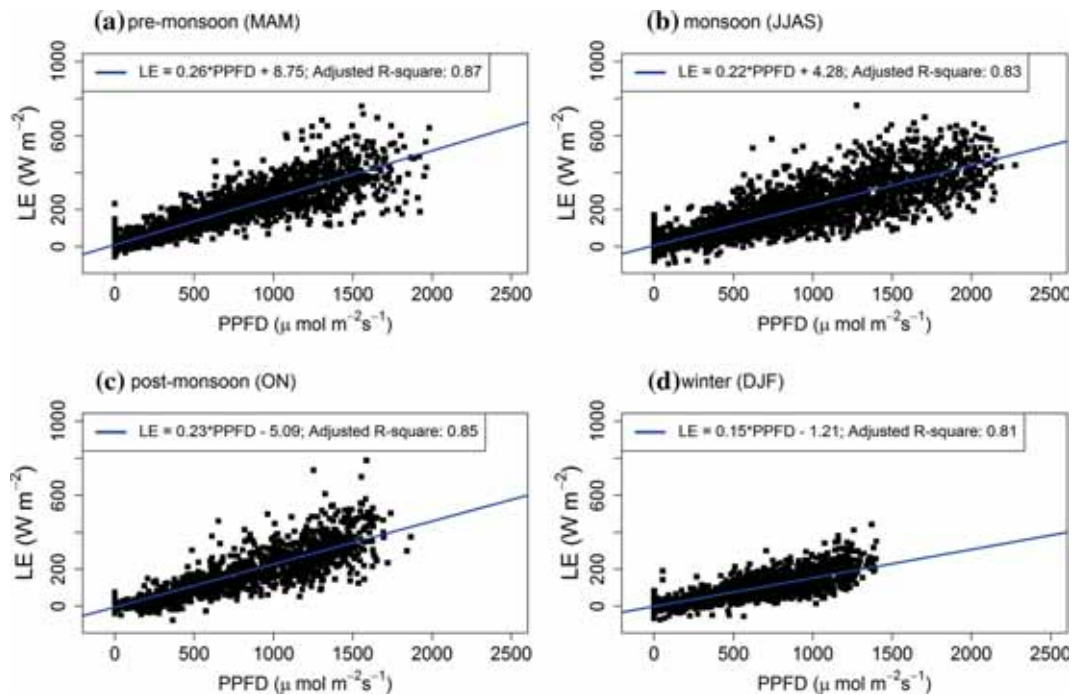
Figure 10. Scatter plots and linear fits between PPFD and LE during (**a**) pre-monsoon (MAM), (**b**) monsoon (JJAS), (**c**) post-monsoon (ON) and (**d**) winter (DJF) at KNP during 2016. Blue lines represent the linear fit between PPFD and LE as obtained by the least-squares method for different seasons. Regression equations and determination coefficients are provided on each panel.

lowest (62%) SEB closures are obtained during pre-monsoon and winter (figure 9), respectively. Intermediate SEB closure is observed during the monsoon (68%) and post-monsoon (72%). Residual energy that is partitioned into $(H + \mathrm{LE})$ but unaccounted in $(R_\mathrm{n}-G)$ is maximum during winter which is 15.55 W m^{-2}. It is comparable to post-monsoon when residual energy remains at 15.36 W m^{-2}. However, this residual energy is minimum at 5.11 W m^{-2} during the monsoon. During pre-monsoon, residual energy stands at 8.53 W m^{-2}. Seasonally mean midday β is maximum at 0.93 during winter and minimum at 0.27 during the monsoon, respectively. β has intermediate values of 0.33 and 0.37 during pre-monsoon and post-monsoon, respectively.

The PPFD is one of the major drivers of photosynthesis which is closely coupled with the transpiration by stomatal control mechanism in plants (Sellers 1987). Increased availability of PPFD accelerates the photosynthesis and hence transpiration. In this paper, the ET is not partitioned into evaporation and transpiration. However, the LE is an analogous representation of the ET. In order to get an overall estimate of the seasonal dependence of ET on the PPFD, scatter plots between the half-hourly values of PPFD and LE are plotted in figure 10. Straight lines are fit to these plots and

the corresponding fit parameters are given in the figure.

Atmospheric VPD is another major driver of ET. In order to compare the control exhibited by VPD on ET for different seasons, the scatter plots between half-hourly values of LE and VPD are plotted by season in figure 11. All plots show clear clockwise temporal trends. To explain the role of VPD in the growth of LE, fits are made to the increasing part of these relationships. These fits are also shown in the same figure.

During pre-monsoon, the minimum and maximum recorded values of VPD are 2.5 and 16 hPa, respectively. The minimum value of LE during pre-monsoon is negligible, but non-zero. LE increases to its maximum value of 300 W m^{-2} in a nonlinear fashion until VPD grows up to 13 hPa. VPD increases further to 16 hPa with a continuous nonlinear decrease in LE until 200 W m^{-2}. Furthermore, VPD decreases continually to 3 hPa with an associated nonlinear decrease in LE.

During the monsoon, the minimum and maximum values of VPD are 3 and 15 hPa, respectively. The minimum value of LE is small but positive during this season. This minimum value of LE is observed when VPD is at its minimum. Initially, LE increases linearly to its maximum value with VPD until 13 hPa. VPD records further growth
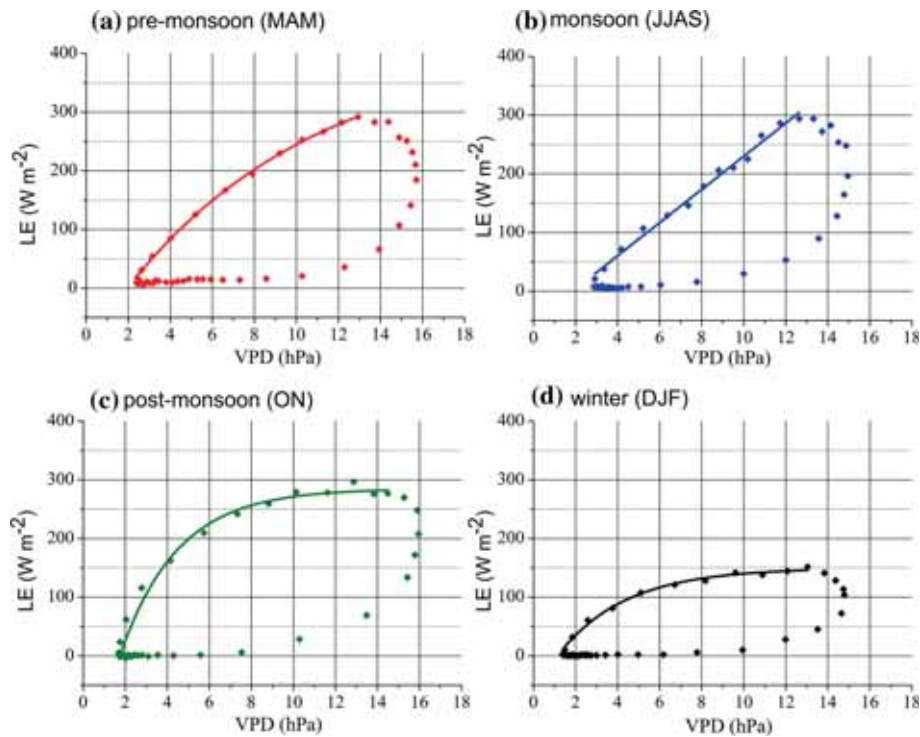
Figure 11. Scatter plots between VPD and LE during (**a**) pre-monsoon (MAM), (**b**) monsoon (JJAS), (**c**) post-monsoon (ON) and (**d**) winter (DJF) in 2016 at KNP. Temporal trend proceeds clockwise in all the plots. Continuous lines represent the fits to the scatter plots during the time when LE increases with VPD.

until 15 hPa beyond this point. During this phase, LE drops to 200 W m^{-2} in a nonlinear fashion. Finally, LE decreases nonlinearly with VPD to their minimum values.

During post-monsoon, the minimum and maximum values of VPD are 1.5 and 16 hPa, respectively. The minimum value of LE during this season is zero. Initially, LE increases nonlinearly with VPD. LE gets saturated at 275 W m^{-2} when VPD reaches 10 hPa. LE maintains this saturation value with a further increase in VPD, until 14 hPa. LE starts decreasing with VPD beyond this value. VPD grows until 16 hPa with an associated continuous decrease in LE until 200 W m^{-2}. LE further decreases nonlinearly with VPD to their minimum values.

In the season of winter, minimum and maximum values of VPD are 1 and 15 hPa, respectively. Initially, LE records a nonlinear growth with VPD. LE gets saturated to 150 W m^{-2} when VPD becomes 10 hPa. This saturation value of LE is maintained until VPD reaches 13 hPa. VPD further grows to 15 hPa during which a continuous nonlinear decrease is observed in LE. Finally, LE decreases with VPD in a nonlinear fashion to the minimum value.

Initially in all seasons, LE is seen to increase with VPD. Gradually, LE reaches the maximum value beyond which it starts decreasing. LE always decreases with decreasing VPD. It has a very nonlinear effect on LE due to two related but contrasting mechanisms. VPD is the pressure difference felt by the water vapour within the plant body with respect to the outside atmosphere. This pressure difference drives the transport of the water vapour through the plant body and eventually its release into the atmosphere through the stomata in the form of transpiration; hence, the more the VPD, the more the LE. On the other hand, a higher VPD inhibits stomatal conductance. This is a negative effect resulting in the stomatal closure and a lower LE. At lower values of VPD, the positive effect remains stronger (Bréda 2003). Hence, LE increases with VPD. Eventually, LE reaches a maximum value after which it starts decreasing. This decreasing effect is due to the strong control of VPD on stomatal conductance at higher values (Gu *et al.* 2005). However, the critical value of VPD at which this transition happens is not fixed and depends on multiple meteorological variables.

4. Discussion

In this work, we aimed to study the seasonal variation of SEB closure at a tropical forest over

north-east India and to improve the imbalance using a simple parameterisation scheme of G. We also studied the role of ET on the surface energy balance during different seasons. We have parameterised G from R_n assuming a linear relationship. Averaged over a daily scale, the net heat flux from the ground is often close to zero. It translates to the fact that heat gain by the soil during daytime is near exactly balanced by the heat loss during night. Additionally, as the soil has very poor heat capacity, net change in the heat stored in the soil during a day is zero (Stull 2012). G constitutes a larger portion of R_n during night-time compared to daytime. This is the manifestation of the fact that H and LE are much smaller during night-time compared to daytime. Hence, more energy is partitioned into G during night-time and daytime and night-time relations between G and R_n are treated separately. As shown earlier, 3.2% of R_n is partitioned into G as compared to 2.5% during daytime. During night-time, incoming shortwave and longwave radiations (R_{SW}(in) and R_{LW}(in), respectively) are absent. However, the Earth loses heat by outgoing longwave radiation (R_{LW}(out)) which results in the cooling of the ground. This is also evident from the negative values of R_n during night-time. Due to poor heat retentivity, the ground loses heat and gets cooler as night progresses. In other words, R_n is driven at the cost of G. Hence, a negative slope between G and R_n is seen during night-time.

The half-hourly values of G, gap-filled by interpolating the linear dependence on R_n, enhance the SEB closure by 1%. To date, a complete closure of SEB using half-hourly values measured from EC and other supportive measurements could not be achieved by the scientific community (Aubinet *et al.* 2012). Typically, 70–90% closure is reported by various flux measurement groups over multiple different ecosystems and terrains across the globe (Anderson *et al.* 2000; Wilson *et al.* 2002; Leuning *et al.* 2012). Over a mixed deciduous forest plantation at Haldwani, Watham *et al.* (2014) report the SEB closure to vary approximately within 60–80% among different months without considering G during a 9-month long observation from January to September 2013. Many corrections have been proposed for improving the estimates from high-frequency EC measurements, resulting in very little or no improvement. It is assumed that this non-closure of SEB has little to do with the post-processing techniques associated with the EC as rectifications proposed for the EC flux measurement have reached the maximum level of accuracy

(Mauder and Foken 2006). SEB often results in a better closure, if calculated on a larger temporal scale (Jarvis *et al.* 1997; Sakai *et al.* 2001). In the present work, daily-averaged values of R_n, H, LE and G are seen to result in 80% closure of SEB. Thus, there is a 10% enhancement in SEB closure. Erroneous estimation of SEB components is also seen to reduce to 0.04 W m^{-2} on a daily scale, from 10.36 W m^{-2} on a half-hourly scale. Clearly, a 259-time improvement in the estimation of SEB components is indicated.

A distinct change in the vegetation cover is observed among the different seasons at the semi-deciduous forest at KNP. The leaf area index (LAI) value increases from a minimum of 0.75 in winter to a maximum of 3.25 during the monsoon season (Deb Burman *et al.* 2017). Gradually increasing and decreasing trends are observed in LAI during pre-monsoon and post-monsoon, respectively. Changes in LAI have a deep impact on transpiration by the forest canopy (Bréda 2003; Wang and Dickinson 2012). Additionally, annual maximum R_n is 550 W m^{-2} observed during this season (figure 8). It decreases in the post-monsoon season and reaches the minimum at 400 W m^{-2} in winter to increase subsequently in the pre-monsoon.

Combined together, these features result in enhanced LE during the monsoon. More R_n is partitioned into LE as is evident from figure 8. Winter is dry over KNP. Maximum LE during this season is 150 W m^{-2} which is half of the maximum LE during the monsoon. Additionally, in winter, LE drops to zero during night-time which is not the case in the monsoon season. On the other hand, H is maximum at 140 W m^{-2} in winter and minimum at 80 W m^{-2} in the monsoon season. Hence, it can be seen that the share of LE in R_n is maximum in the monsoon season and minimum in winter. This is supported by a study by Brümmer *et al.* (2008) in which the differential responses of shrub savanna during dry and wet seasons were studied. The proportion of LE in R_n increases during pre-monsoon as the moisture-laden air starts entering the landmass. In contrast, it decreases during post-monsoon as this moist airmass gradually recedes from the landmass.

These observations suggest that SEB closure needs to be carefully examined for each season as the relative strengths of different SEB components vary widely from one season to another. These changes are brought in by different physical, dynamical and physiological processes which may not be resolved on an annual scale (Ramier *et al.*

2009). As seen in the present work, the best and the worst closures of SEB are 76% and 62% which are observed during the pre-monsoon and winter, respectively. Intermediate closures of 68% and 72% are seen in the monsoon and post-monsoon seasons, respectively. Residual energy is the minimum in the monsoon season at 5.11 W m^{-2}, and maximum in winter and the post-monsoon at 15.55 and 15.36 W m^{-2}, respectively. Residual energy during the pre-monsoon season remains at 8.53 W m^{-2}. These observations show that with the least ET happening, the worst closure is achieved during winter which also increases the magnitude of residual energy. This can be explained as follows. During winter, a significant proportion of R_n gets channelised into other components which cannot be directly measured and hence are not included in SEB. Such components may include canopy storage, absorbed radiation, etc. (Aubinet *et al.* 2012). These losses in R_n are reflected as the residual energy.

On the other hand, with more ET happening during the monsoon season, a major chunk of R_n is partitioned into LE which is measured with good confidence (Mauder and Foken 2006; Foken *et al.* 2011). This brings down the residual energy that accounts for the various losses. As a result, better SEB closure is observed in the monsoon season. Both pre-monsoon and post-monsoon are the transitioning phases between monsoon and winter with the difference being the gradual increase and decrease in the temperature of the atmospheric air column. This can be seen from the greater magnitude of H during pre-monsoon over post-monsoon. LE is similar to that in the monsoon climate in both of these seasons. With more R_n being partitioned into LE, SEB closures better than in winter are observed in these two seasons. A seasonal variation of residual energy has the same pattern as β as seen from table 3. Maximum and minimum values of β result in the largest and smallest values of the residual energy, respectively. It suggests that the closure of SEB is linked with the relative partitioning of energy between H and LE: the more the value of LE, the lesser the value of β, and hence, the better the SEB closure. Hence, ET is seen to have a decisive role in the variation of the SEB closure among different seasons.

In order to further investigate the role of LE in the SEB closure, the relation between LE and PPFD in different seasons has been studied. However, LE has not been separated into evaporation and transpiration as our objective in this study

remains not to study the interrelationship between these two which is a complex biogeochemical process (Lawrence *et al.* 2007) but to assess their combined impact on SEB among different seasons. LE increases with PPFD during all seasons. Increased PPFD results in enhanced photosynthetic activity in plants (Frolking *et al.* 1998; Reverter *et al.* 2010). This in turn triggers transpiration as it is closely coupled with photosynthesis (Wang *et al.* 2006). Linear fits between LE and PPFD have adjusted R-square values of 0.87, 0.83, 0.85 and 0.81 during pre-monsoon, monsoon, post-monsoon and winter, respectively. Similar findings have been reported by Greco and Baldocchi (1996) and Pieruschka *et al.* (2010) where transpiration changed proportionately with PPFD. The slope between LE and PPFD remains similar during pre-monsoon, monsoon and post-monsoon which are 0.26, 0.22 and 0.23, respectively. However, it is markedly different at 0.15 during winter. Being deciduous, the forest at KNP sheds leaves during winter. This is evident from the LAI value of the canopy which drops down to a mere 0.75 in winter from 3.25 in the monsoon season (Deb Burman *et al.* 2017). Hence, during winter, an increase in PPFD does not increase transpiration much. That is why the PPFD has overall less control on ET.

Marked differences are found in the pattern of variation of LE with VPD among different seasons at KNP. In all seasons, LE grows initially with VPD during daytime. However, it starts decreasing after VPD reaches a critical value. On the other hand, LE decreases monotonically in a nonlinear fashion with VPD during night-time during all seasons. Such type of behaviour exhibits a clear hysteresis pattern quite similar to the one reported by Hogg and Hurdle (1997) and Gyenge *et al.* (2003). The growth of LE at lower values of VPD can be attributed to enhanced transpiration as explained by Gu *et al.* (2006). However, after a critical value of VPD, stomatal closure takes place in plants causing the cessation of sap flow (Anthoni *et al.* 2002; Fisher *et al.* 2007). As a result of this, transpiration saturates and eventually starts decreasing. KNP being a densely vegetated tropical forest, transpiration dominates the ET process (Jasechko *et al.* 2013). However, during the monsoon atmosphere becomes significantly more humid than the other times of the year. As a result, evaporation is stronger in the monsoon season than in the three other seasons. This is seen from the minimum values of VPD observed in different seasons. During the monsoon, VPD never falls below 3 hPa,

whereas in winter, it reaches as low as 1 hPa. Annually, minimum and maximum VPD are observed in winter and post-monsoon, which are 1 and 16 hPa, respectively. Due to the increased availability of moisture in monsoon, LE records a linear growth with VPD as seen from figure 11(b). Similar behaviour has been found by Goldstein *et al.* (2000) and Admiral *et al.* (2006). Being a deciduous forest, KNP records the lowest annual LAI in winter (Deb Burman *et al.* 2017). It is also the driest period of the year as the available moisture content in the atmosphere remains the lowest in this season. As a result, both evaporation and transpiration are hindered. Hence, LE saturates to the lowest value in winter among all four seasons. With the advent of monsoonal wind rich in water vapour, a gradual increase in atmospheric moisture content is observed in the pre-monsoon season. Moreover, increased LAI is observed during this time at KNP due to the growth of new leaves (Deb Burman *et al.* 2017). Hence, LE grows with VPD at a faster rate during this season due to the increased combination of both evaporation and transpiration. Finally, after reaching the critical value, it decreases due to stomatal closure (Gyenge *et al.* 2003). On the other hand, a withdrawal of the monsoonal wind happens in the post-monsoon season, resulting in the gradual decrease of moisture content in the atmosphere. LAI also starts to decrease during post-monsoon (Deb Burman *et al.* 2017). As a result, ET is hindered and, hence, does not increase with VPD. This is manifested in the saturation of LE with VPD. During night-time in all seasons, convective activities reduce in the absence of solar heating. Sap flow also reduces in plants, bringing the transpiration down. As a combined effect of both, LE decreases monotonically with VPD during night-time.

5. Conclusions

The seasonal variation of SEB has been studied for the first time in a tropical forest over north-east India using a year-round ground-based observation of meteorological variables and EC fluxes during 2016. SEB closure is seen to vary widely among different seasons with the maximum closure of 76% in the pre-monsoon season and the minimum closure of 62% in winter. During the Indian summer monsoon, a closure of 68% is recorded, while a 72% closure is observed post-monsoon. The annual closure obtained was 70% and 80% using half-hourly and daily values, respectively. ET plays an important role in the closure process. The closure of SEB is seen to be linked with the relative strengths of the sensible and LEs. The worst closure is observed at the highest value of Bowen ratio, during winter and the best closure is observed at the smallest value of Bowen ratio in the monsoon season. PPFD and VPD exhibit close controls on ET which vary markedly among different seasons. In order to gain a deeper understanding of the controls of ET, we plan to classify it into evaporation and transpiration and subsequently study the effects of meteorological, radiation and soil parameters on both these processes separately in our future studies.

References

Admiral S W, Lafleur P M and Roulet N T 2006 Controls on latent heat flux and energy partitioning at a peat bog in eastern Canada; *Agric. For. Meteorol.* **140** 308–321, https://doi.org/10.1016/j.agrformet.2006.03.017.

Anderson M C, Norman J M, Meyers T P and Diak G R 2000 An analytical model for estimating canopy transpiration and carbon assimilation fluxes based on canopy light-use efficiency; *Agric. For. Meteorol.* **101** 265–289, https://doi.org/10.1016/S0168-1923(99)00170-7.

Anthoni P M, Unsworth M H, Law B E, Irvine J, Baldocchi D D, Van Tuyl S and Moore D 2002 Seasonal differences in carbon and water vapor exchange in young and old-growth ponderosa pine ecosystems; *Agric. For. Meteorol.* **111** 203–222, https://doi.org/10.1016/S0168-1923(02)00021-7.

Aubinet M, Vesala T and Papale D 2012 *Eddy covariance: A practical guide to measurement and data analysis*; Springer, New York, https://doi.org/10.1007/978-94-007-2351-1.

Baldocchi D 2014 Measuring fluxes of trace gases and energy between ecosystems and the atmosphere – the state and future of the eddy covariance method; *Global Chang. Biol.* **20** 3600–3609, https://doi.org/10.1111/gcb.12649.

Baldocchi D, Falge E, Gu L and Olson R *et al.* 2001 FLUXNET: A new tool to study the temporal and spatial variability of ecosystem-scale carbon dioxide, water vapor, and energy flux densities; *Bull. Am. Meteorol. Soc.* **82**, 2415, https://doi.org/10.1175/1520-0477(2001)082<2415:FANTTS>2.3.CO;2.

Bhat G S and Arunchandra S C 2009 On the measurement of the surface energy budget over a land surface during the summer monsoon; *J. Earth Syst. Sci.* **117** 911–923, https://doi.org/10.1007/s12040-008-0076-0.

Bhat G S and Narasimha R 2007 Indian summer monsoon experiments; *Curr. Sci.* **93** 153–164.

Bovard B D, Curtis P S, Vogel C S, Su H-B and Schmid H P 2005 Environmental controls on sap flow in a northern hardwood forest; *Tree Physiol.* **25** 31–38, https://doi.org/10.1093/treephys/25.1.31.

Bréda N J J 2003 Ground-based measurements of leaf area index: A review of methods, instruments and current controversies; *J. Exp. Bot.* **54** 2403–2417, https://doi.org/10.1093/jxb/erg263.

Brümmer C, Falk U, Papen H, Szarzynski J, Wassmann R and Brüggemann N 2008 Diurnal, seasonal, and interannual variation in carbon dioxide and energy exchange in shrub savanna in Burkina Faso (West Africa); *J. Geophys. Res. Atmos.* **113,** https://doi.org/10.1029/2007JG000583.

Burba G 2013 *Eddy covariance method for scientific, industrial, agricultural and regulatory applications: A field book on measuring ecosystem gas exchange and areal emission rates*; LI-Cor Biosciences, Lincoln, NE, 331p.

Caird M A, Richards J H and Donovan L A 2007 Nighttime stomatal conductance and transpiration in C3 and C4 plants; *Plant Physiol.* **143** 4–10, https://doi.org/10.1104/pp.106.092940

Chatterjee A, Roy A, Chakraborty S, Karipot A K, Sarkar C, Singh S, Ghosh S K, Mitra A and Raha S 2018 Biosphere atmosphere exchange of CO_2, H_2O vapour and energy during spring over a high altitude Himalayan Forest at Eastern India; *Aerosol. Air Qual. Res.*, https://doi.org/10.4209/aaqr.2017.12.0605.

Cho J, Oki T, Yeh P J-F, Kim W, Kanae S and Otsuki K 2012 On the relationship between the Bowen ratio and the near-surface air temperature; *Theor. Appl. Climatol.* **108** 135–145, https://doi.org/10.1007/s00704-011-0520-y.

Daughtry C S T, Kustas W P, Moran M S, Pinter P J, Jackson R D, Brown P W, Nichols W D and Gay L W 1990 Spectral estimates of net radiation and soil heat flux; *Remote Sens. Environ.* **32** 111–124, https://doi.org/10.1016/0034-4257(90)90012-B.

Dawson T E, Burgess S S O, Tu K P, Oliveira R S, Santiago L S, Fisher J B, Simonin K A and Ambrose A R 2007 Night-time transpiration in woody plants from contrasting ecosystems; *Tree Physiol.* **27** 561–575, https://doi.org/10.1093/treephys/27.4.561.

Deb Burman P K, Sarma D, Williams M, Karipot A and Chakraborty S 2017 Estimating gross primary productivity of a tropical forest ecosystem over north-east India using LAI and meteorological variables; *J. Earth Syst. Sci.* **126** 1–16, https://doi.org/10.1007/s12040-017-0874-3.

de Silans A P, Monteny B A and Lhomme J P 1997 The correction of soil heat flux measurements to derive an accurate surface energy balance by the Bowen ratio method; *J. Hydrol.* **188** 453–465, https://doi.org/10.1016/S0022-1694(96)03187-3.

Dirmeyer P A, Gao X, Zhao M, Guo Z, Oki T and Hanasaki N 2006 GSWP-2: Multimodel analysis and implications for our perception of the land surface; *Bull.*

Am. Meteorol. Soc. **87** 1381–1397, https://doi.org/10.1175/BAMS-87-10-1381.

Dugas W A, Fritschen L J, Gay L W, Held A A, Matthias A D, Reicosky D C, Steduto P and Steiner J L 1991 Bowen ratio, eddy correlation, and portable chamber measurements of sensible and latent heat flux over irrigated spring wheat; *Agric. For. Meteorol.* **56** 1–20, https://doi.org/10.1016/0168-1923(91)90101-U.

Eamus D, Hutley L B and O'Grady A P 2001 Daily and seasonal patterns of carbon and water fluxes above a north Australian savanna; *Tree Physiol.* **21** 977–988, https://doi.org/10.1093/treephys/21.12-13.977.

Finkelstein P L and Sims P F 2001 Sampling error in eddy correlation flux measurements; *J. Geophys. Res.*, https://doi.org/10.1029/2000JD900731.

Fisher J B, Baldocchi D D, Misson L, Dawson T E and Goldstein A H 2007 What the towers don't see at night: Nocturnal sap flow in trees and shrubs at two AmeriFlux sites in California; *Tree Physiol.* **27** 597–610, https://doi.org/10.1093/treephys/27.4.597.

Fisher R A, Williams M, de Lourdes Ruivo M, de Costa A L and Meir P 2008 Evaluating climatic and soil water controls on evapotranspiration at two Amazonian rainforest sites; *Agric. For. Meteorol.* **148** 850–861, https://doi.org/10.1016/j.agrformet.2007.12.001.

Fisher J B, Malhi Y, Bonal D, Da Rocha H R, De Araujo A C, Gamo M, Goulden M L, Hirano T, Huete A R and Kondo H, *et al.* 2009 The land–atmosphere water flux in the tropics; *Glob. Chang. Biol.* **15** 2694–2714, https://doi.org/10.1111/j.1365-2486.2008.01813.x.

Foken T, Göockede M, Mauder M, Mahrt L, Amiro B and Munger W 2004 Post-field data quality control; In: *Handbook of micrometeorology. Atmospheric and oceanographic sciences library* (eds) Lee X, Massman W, Law B, Vol. **29**, Springer, Dordrecht, https://doi.org/10.1007/1-4020-2265-4_9.

Foken T, Aubinet M, Finnigan J J, Leclerc M Y, Mauder M and Kyaw Tha Paw U 2011 Results of a panel discussion about the energy balance closure correction for trace gases; *Bull. Am. Meteorol. Soc.* **92** ES13–ES18, https://doi.org/10.1175/2011BAMS3130.1.

Frolking S E *et al.* 1998 The relationship between ecosystem productivity and photosynthetically active radiation for northern peatlands; *Global Biogeochem. Cycles* **12** 115–126.

Gadgil S and Gadgil S 2006 The Indian monsoon, GDP and agriculture; *Econ. Polit. Wkly.* **41** 4887–4895, https://doi.org/10.2307/4418949.

Giambelluca T W, Martin R E, Asner G P, Huang M, Mudd R G, Nullet M A, DeLay J K and Foote D 2009 Evapotranspiration and energy balance of native wet montane cloud forest in Hawai'i; *Agric. For. Meteorol.* **149** 230–243, https://doi.org/10.1016/j.agrformet.2008.08.004.

Gnanamoorthy P, Selvam V, Ramasubramanian R, Nagarajan R, Chakraborty S, Deb Burman P K and Karipot A 2019 Diurnal and seasonal patterns of soil CO_2 efflux from the Pichavaram mangroves, India; *Environ. Monit. Assess.* **191** 1–12. https://doi.org/10.1007/s10661-019-7407-2.

Goldstein A H, Hultman N E, Fracheboud J M, Bauer M R, Panek J A, Xu M, Qi Y, Guenther A B and Baugh W 2000 Effects of climate variability on the carbon dioxide, water,

and sensible heat fluxes above a ponderosa pine plantation in the Sierra Nevada (CA); *Agric. For. Meteorol.* **101** 113–129, https://doi.org/10.1016/S0168-1923(99)00168-9.

Goswami B N and Ajayamohan R S 2001 Intraseasonal oscillations and interannual variability of the Indian summer monsoon; *J. Clim.* **14** 1180–1198, https://doi.org/10.1175/1520-0442(2001)014<1180:IOAIVO>2.0.CO;2.

Greco S and Baldocchi D D 1996 Seasonal variations of CO_2 and water vapour exchange rates over a temperate deciduous forest; *Glob. Chang. Biol.* **2** 183–197, https://doi.org/10.1111/j.1365-2486.1996.tb00071.x.

Gu S, Tang Y, Cui X, Kato T, Du M, Li Y and Zhao X 2005 Energy exchange between the atmosphere and a meadow ecosystem on the Qinghai–Tibetan Plateau; *Agric. For. Meteorol.* **129** 175–185, https://doi.org/10.1016/j.agrformet.2004.12.002.

Gu L, Meyers T, Pallardy S G, Hanson P J, Yang B, Heuer M, Hosman K P, Riggs J S, Sluss D and Wullschleger S D 2006 Direct and indirect effects of atmospheric conditions and soil moisture on surface energy partitioning revealed by a prolonged drought at a temperate forest site; *J. Geophys. Res. Atmos.* **111**, 1–13, https://doi.org/10.1029/2006JD007161.

Gyenge J E, Fernández M E and Schlichter T M 2003 Water relations of ponderosa pines in Patagonia Argentina: Implications for local water resources and individual growth; *Trees-structure Funct.* **17** 417–423, https://doi.org/10.1007/s00468-003-0254-2.

Heusinkveld B G, Jacobs A F G, Holtslag A A M and Berkowicz S M 2004 Surface energy balance closure in an arid region: Role of soil heat flux; *Agric. For. Meteorol.* **122** 21–37, https://doi.org/10.1016/j.agrformet.2003.09.005.

Hingane L S, Rupa Kumar K and Ramana Murty B V 1985. Long-term trends of surface air temperature in India; *J. Climatol.* **5** 521–528, https://doi.org/10.1002/joc.3370050505.

Hogg E H and Hurdle P A 1997 Sap flow in trembling aspen: Implications for stomatal responses to vapor pressure deficit; *Tree Physiol.* **17** 501–509, https://doi.org/10.1093/treephys/17.8-9.501.

Idso S B, Aase J K and Jackson R D 1975 Net radiation – Soil heat flux relations as influenced by soil water content variations; *Bound.-Layer Meteorol.* **9** 113–122, https://doi.org/10.1007/BF00232257.

Jain S K and Kumar V 2012 Trend analysis of rainfall and temperature data for India; *Curr. Sci.* **102** 37–49.

Jarvis P G, Massheder J M, Hale S E, Moncrieff J B, Rayment M and Scott S L 1997 Seasonal variation of carbon dioxide, water vapor, and energy exchanges of a boreal black spruce forest; *J. Geophys. Res. Atmos.* **102** 28953–28966, https://doi.org/10.1029/97JD01176.

Jasechko S, Sharp Z D, Gibson J J, Birks S J, Yi Y and Fawcett P J 2013 Terrestrial water fluxes dominated by transpiration; *Nature* **496** 347–350, https://doi.org/10.1038/nature11983.

Jha C S, Thumaty K C, Rodda S R, Sonakia A and Dadhwal V K 2013 Analysis of carbon dioxide, water vapour and energy fluxes over an Indian teak mixed deciduous forest for winter and summer months using eddy covariance technique; *J. Earth Syst. Sci.* **122** 1259–1268, https://doi.org/10.1007/s12040-013-0350-7.

Jhajharia D, Shrivastava S K, Sarkar D and Sarkar S 2009 Temporal characteristics of pan evaporation trends under the humid conditions of northeast India; *Agric. For. Meteorol.* **149** 763–770, https://doi.org/10.1016/j.agrformet.2008.10.024.

Jung M, Reichstein M, Margolis H A, Cescatti A, Richardson A D, Arain M A, Arneth A, Bernhofer C, Bonal D and Chen J *et al.* 2011 Global patterns of land-atmosphere fluxes of carbon dioxide, latent heat, and sensible heat derived from eddy covariance, satellite, and meteorological observations; *J. Geophys. Res. Biogeosci.* **116**, https://doi.org/10.1029/2010JG001566.

Kaimal J C and Finnigan J J 1994 *Atmospheric boundary layer flows: Their structure and measurement*; Oxford University Press.

Kool D, Agam N, Lazarovitch N, Heitman J L, Sauer T J and Ben-Gal A 2014 A review of approaches for evapotranspiration partitioning; *Agric. For. Meteorol.* **184** 56–70, https://doi.org/10.1016/j.agrformet.2013.09.003.

Kottek M, Grieser J, Beck C, Rudolf B and Rubel F 2006 World map of the Köppen-Geiger climate classification updated; *Meteorol. Zeitschrift* **15** 259–263, https://doi.org/10.1127/0941-2948/2006/0130.

Kustas W P and Daughtry C S T 1990 Estimation of the soil heat flux/net radiation ratio from spectral data; *Agric. For. Meteorol.* **49** 205–223, https://doi.org/10.1016/0168-1923(90)90033-3.

Kustas W P, Daughtry C S T and Van Oevelen P J 1993 Analytical treatment of the relationships between soil heat flux/net radiation ratio and vegetation indices; *Remote Sens. Environ.* **46** 319–330, https://doi.org/10.1016/0034-4257(93)90052-Y.

Lawrence D M, Thornton P E, Oleson K W and Bonan G B 2007 The partitioning of evapotranspiration into transpiration, soil evaporation, and canopy evaporation in a GCM: Impacts on land–atmosphere interaction; *J. Hydrometeorol.* **8** 862–880, https://doi.org/10.1175/JHM596.1.

Leuning R, Van Gorsel E, Massman W J and Isaac P R 2012 Reflections on the surface energy imbalance problem; *Agric. For. Meteorol.* **156** 65–74, https://doi.org/10.1016/j.agrformet.2011.12.002.

Malek E and Bingham G E 1993 Comparison of the Bowen ratio-energy balance and the water balance methods for the measurement of evapotranspiration; *J. Hydrol.* **146** 209–220, https://doi.org/10.1016/0022-1694(93)90276-F.

Mauder M and Foken T 2006 Impact of post-field data processing on eddy covariance flux estimates and energy balance closure; *Meteorol. Zeitschrift* **15** 597–609, https://doi.org/10.1127/0941-2948/2006/0167.

Mauder M, Cuntz M, Drüe C, Graf A, Rebmann C, Schmid H P, Schmidt M and Steinbrecher R 2013 A strategy for quality and uncertainty assessment of long-term eddy-covariance measurements; *Agric. For. Meteorol.* **169** 122–135, https://doi.org/10.1016/j.agrformet.2012.09.006.

Moffat A M, Papale D, Reichstein M, Hollinger D Y, Richardson A D, Barr A G, Beckstein C, Braswell B H, Churkina G and Desai A R, *et al.* 2007 Comprehensive comparison of gap-filling techniques for eddy covariance net carbon fluxes; *Agric. For. Meteorol.* **147** 209–232, https://doi.org/10.1016/j.agrformet.2007.08.011.

Moncrieff J B, Massheder J M, de Bruin H, Elbers J, Friborg T, Heusinkveld B, Kabat P, Scott S, Soegaard H and Verhoef A 1997 A system to measure surface fluxes of momentum, sensible heat, water vapour and carbon dioxide; *J. Hydrol.* **188–189** 589–611, https://doi.org/10.1016/S0022-1694(96)03194-0.

Moncrieff J, Clement R, Finnigan J and Meyers T 2004 Averaging, detrending, and filtering of eddy covariance time series; In: *Handbook of micrometeorology. Atmospheric and oceanographic sciences library* (eds) Lee X, Massman W, Law B, Vol **29**, Springer, Dordrecht, https://doi.org/10.1007/1-4020-2265-4_2

Monteith J L 1965 Evaporation and the environment; In: *The state and movement of water in living organisms* (ed.) Fogg G E, *Symposium of the Society of Experimental Biology*, Vol. **19**, Cambridge University Press, London.

Mukhopadhyay P, Jaswal A and Deshpande M 2017 Variability and trends of atmospheric moisture over the Indian region; In: *Observed climate variability and change over the Indian region* (eds) Rajeevan M and Nayak S, Springer, Singapore, pp. 129–144, https://doi.org/10.1007/978-981-10-2531-0_8.

Nakai T, der Molen M K, Gash J H C and Kodama Y 2006 Correction of sonic anemometer angle of attack errors; *Agric. For. Meteorol.* **136** 19–30, https://doi.org/10.1016/j.agrformet.2006.01.006.

Norman J M, Kustas W P, Prueger J H and Diak G R 2000 Surface flux estimation using radiometric temperature: A dual temperature-difference method to minimize measurement errors; *Water Resour. Res.* **36** 2263–2274, https://doi.org/10.1029/2000wr900033.

Novick K A, Oren R, Stoy P C, Siqueira M B S and Katul G G 2009 Nocturnal evapotranspiration in eddy-covariance records from three co-located ecosystems in the Southeastern US: Implications for annual fluxes; *Agric. For. Meteorol.* **149** 1491–1504, https://doi.org/10.1016/j.agrformet.2009.04.005.

Papale D, Reichstein M, Aubinet M, Canfora E, Bernhofer C, Kutsch W, Longdoz B, Rambal S, Valentini R and Vesala T, *et al.* 2006 Towards a standardized processing of net ecosystem exchange measured with eddy covariance technique: Algorithms and uncertainty estimation; *Biogeosciences* **3** 571–583, https://doi.org/10.5194/bg-3-571-2006.

Parthasarathy B, Rupa Kumar K and Sontakke N A 1990 Surface and upper air temperatures over India in relation to monsoon rainfall; *Theor. Appl. Climatol.* **42** 93–110, https://doi.org/10.1007/BF00868216.

Parthasarathy B, Munot A A and Kothawale D R 1994 All-India monthly and seasonal rainfall series: 1871–1993; *Theor. Appl. Climatol.* **49** 217–224, https://doi.org/10.1007/BF00867461.

Pejam M R, Arain M A and McCaughey J H 2006 Energy and water vapour exchanges over a mixed wood boreal forest in Ontario, Canada; *Hydrol. Process.* **20** 3709–3724, https://doi.org/10.1002/hyp.6384.

Pieruschka R, Huber G and Berry J A 2010 Control of transpiration by radiation; *Proc. Natl. Acad. Sci.* **107** 13372–13377, https://doi.org/10.1073/pnas.0913177107.

Purdy A J, Fisher J B, Goulden M L and Famiglietti J S 2016 Ground heat flux: An analytical review of 6 models evaluated at 88 sites and globally; *J. Geophys. Res. Biogeosci.* **121** 3045–3059, https://doi.org/10.1002/2016JG003591.

Ramana M V, Krishnan P and Kunhikrishnan P K 2004 Surface boundary-layer characteristics over a tropical inland station: Seasonal features; *Boundary-Layer Meteorol.* **111** 153–175. https://doi.org/10.1023/B:BOUN.0000010999.25921.1a

Ramier D, Boulain N, Cappelaere B, Timouk F, Rabanit M, Lloyd C R, Boubkraoui S, Métayer F, Descroix L and Wawrzyniak V 2009 Towards an understanding of coupled physical and biological processes in the cultivated Sahel–1. Energy Water; *J. Hydrol.* **375** 204–216, https://doi.org/10.1016/j.jhydrol.2008.12.002.

Randerson J T, Chapin F S, Harden J W, Neff J C and Harmon M E 2002 Net ecosystem production: A comprehensive measure of net carbon accumulation by ecosystems; *Ecol. Appl.* **12** 937–947, https://doi.org/10.1890/1051-0761(2002)012[0937:NEPACM]2.0.CO;2.

Reddy N N and Rao K G 2018 Contrasting variations in the surface layer structure between the convective and non-convective periods in the summer monsoon season for Bangalore location during PRWONAM; *J. Atmos. Sol.-Terr. Phys.* **167** 156–168, https://doi.org/10.1016/j.jastp.2017.11.017.

Reichstein M, Falge E, Baldocchi D, Papale D, Aubinet M, Berbigier P, Bernhofer C, Buchmann N, Gilmanov T and Granier A, *et al.* 2005 On the separation of net ecosystem exchange into assimilation and ecosystem respiration: Review and improved algorithm; *Glob. Chang. Biol.* **11** 1424–1439, https://doi.org/10.1111/j.1365-2486.2005.001002.x.

Reverter B R, Sánchez-Cañete E P, Resco V, Serrano-Ortiz P, Oyonarte C and Kowalski A S 2010 Analyzing the major drivers of NEE in a Mediterranean alpine shrubland; *Biogeosciences* **7** 2601–2611, https://doi.org/10.5194/bg-7-2601-2010.

Rodda S R, Thumaty K C, Jha C S and Dadhwal V K 2016 Seasonal variations of carbon dioxide, water vapor and energy fluxes in Tropical Indian Mangroves; *Forests* **7** 35, https://doi.org/10.3390/f7020035.

Rothfuss Y, Biron P, Braud I, Canale L, Durand J, Gaudet J, Richard P, Vauclin M and Bariac T 2010 Partitioning of evapotranspiration into soil evaporation and plant partitioning evapotranspiration fluxes into soil evaporation and plant transpiration using water stable isotopes under controlled conditions; *Hydrol. Process.* **24** 3177–3194, https://doi.org/10.1002/hyp.7743.

Sachs L 1997 *Angewandte statistik: Anwendung statistischer methoden*; Springer, Berlin.

Sakai R K, Fitzjarrald D R and Moore K E 2001 Importance of low-frequency contributions to eddy fluxes observed over rough surfaces; *J. Appl. Meteorol.* **40** 2178–2192.

Sauer T J, Ochsner T E and Horton R 2007 Soil heat flux plates; *Agron. J.* **99** 304–310, https://doi.org/10.2134/agronj2005.0038s.

Scott R L, Edwards E A, Shuttleworth W J, Huxman T E, Watts C and Goodrich D C 2004 Interannual and seasonal variation in fluxes of water and carbon dioxide from a riparian woodland ecosystem; *Agric. For. Meteorol.* **122** 65–84, https://doi.org/10.1016/j.agrformet.2003.09.001.

Sellers P J 1987 Canopy reflectance, photosynthesis, and transpiration, II; The role of biophysics in the linearity of their interdependence; *Remote Sens. Environ.* **21** 143–183, https://doi.org/10.1016/0034-4257(87)90051-4.

Shi T-T, Guan D-X, Wu J-B, Wang A-Z, Jin C-J and Han S-J 2008 Comparison of methods for estimating evapotranspiration rate of dry forest canopy: Eddy covariance, Bowen ratio energy balance, and Penman-Monteith equation; *J. Geophys. Res. Atmos.* **113**, https://doi.org/10.1029/2008JD010174.

Shuttleworth W J 2007 Putting the "vap" into evaporation; *Hydrol. Earth Syst. Sci.* **11** 210–244, https://doi.org/10.5194/hess-11-210-2007.

Si J-H, Feng Q, Zhang X-Y, Chang Z-Q, Su Y-H and Xi H 2007 Sap flow of *Populus euphratica* in a desert riparian forest in an extreme arid region during the growing season; *J. Integr. Plant Biol.* **49**, 425–436, https://doi.org/10.1111/j.1744-7909.2007.00388.x.

Sikka D R and Narasimha R 1995 Genesis of the monsoon trough boundary layer experiment (MONTBLEX); *Planet. Sci. (Earth Planet. Sci.)* **104** 157–187, https://doi.org/10.1007/BF02839270.

Singh O P, Ali Khan T M and Rahman M S 2000 Changes in the frequency of tropical cyclones over the North Indian Ocean; *Meteorol. Atmos. Phys.* **75** 11–20, https://doi.org/10.1007/s007030070011.

Stull R B 2012 *An introduction to boundary layer meteorology*; Vol. **13**, Springer, Dordrecht, https://doi.org/10.1007/978-94-009-3027-8.

Tanner C 1960 Energy balance approach to evapotranspiration from crops; *Soil Sci. Soc. Am. J.* **24** 1–9, https://doi.org/10.2136/sssaj1960.03615995002400010012x.

Tsai J-L, Tsuang B-J, Lu P-S, Chang K-H, Yao M-H and Shen Y 2010 Measurements of aerodynamic roughness, Bowen ratio, and atmospheric surface layer height by eddy covariance and tethersonde systems simultaneously over a heterogeneous rice paddy; *J. Hydrometeorol.* **11** 452–466. https://doi.org/10.1175/2009JHM1131.1.

Twine T E, Kustas W P, Norman J M, Cook D R, Houser P, Meyers T P, Prueger J H, Starks P J and Wesely M L 2000 Correcting eddy-covariance flux underestimates over a grassland; *Agric. For. Meteorol.* **103** 279–300, https://doi.org/10.1016/S0168-1923(00)00123-4.

Vernekar K G, Sadani L K, Sivaramakrishnan S, Parasnis S S, Mohan B, Saxena S, Dharmaraj T, Patil M N, Pillai J S, Murthy B S, Debaje S B and Bagavathsingh A 2003 An overview of the land surface processes experiment (LASPEX) over a semi-arid region of India; *Bound.-Layer Meteorol.* **106**(**3**) 561–572, https://doi.org/10.1023/A:1021283503661.

Wang B 2006 *The Asian monsoon*; Springer, Heidelberg, https://doi.org/10.1007/3-540-37722-0.

Wang K and Dickinson R E 2012 A review of global terrestrial evapotranspiration: Observation, modeling, climatology, and climatic variability; *Rev. Geophys.* **50**, 1–54, https://doi.org/10.1029/2011RG000373.

Wang B and Ho L 2002 Rainy season of the Asian-Pacific summer monsoon; *J. Clim.* **15** 386–398, https://doi.org/10.1175/1520-0442(2002)015<0386:RSOTAP>2.0.CO;2.

Wang J, Yu Q, Li J, Li L-H, Li X-G, Yu G-R and Sun X-M 2006 Simulation of diurnal variations of CO_2, water and heat fluxes over winter wheat with a model coupled photosynthesis and transpiration; *Agric. For. Meteorol.* **137** 194–219, https://doi.org/10.1016/j.agrformet.2006.02.007.

Watham T, Kushwaha S P, Patel N R and Dadhwal V K 2014 Monitoring of carbon dioxide and water vapour exchange over a young mixed forest plantation using eddy covariance technique; *Curr. Sci.* **107** 858–866.

Webb E K, Pearman G I and Leuning R 1980 Correction of flux measurements for density effects due to heat and water vapour transfer; *Quart. J. Roy. Meteorol. Soc.* **106** 85–100, https://doi.org/10.1002/qj.49710644707.

Wilson K B and Baldocchi D D 2000 Seasonal and inter-annual variability of energy fluxes over a broadleaved temperate deciduous forest in North America; *Agric. For. Meteorol.* **100** 1–18, https://doi.org/10.1016/S0168-1923(99)00088-X.

Wilson K, Goldstein A, Falge E, Aubinet M, Baldocchi D, Berbigier P, Bernhofer C, Ceulemans R, Dolman H and Field C, *et al.* 2002 Energy balance closure at FLUXNET sites; *Agric. For. Meteorol.* **113** 223–243, https://doi.org/10.1016/S0168-1923(02)00109-0.

Wutzler T, Lucas-Moffat A, Migliavacca M, Knauer J, Sickel K, Šigut L, Menzer O and Reichstein M 2018 Basic and extensible post-processing of eddy covariance flux data with REddyProc; *Biogeosci. Discuss.* **15** 1–39, https://doi.org/10.5194/bg-2018-56.

Xavier P K, Marzin C and Goswami B N 2007 An objective definition of the Indian summer monsoon season and a new perspective on the ENSO-monsoon relationship; *Quart. J. Roy. Meteorol. Soc.* **133** 749–764, https://doi.org/10.1002/qj.45.

Yang K and Wang J 2008 A temperature prediction-correction method for estimating surface soil heat flux from soil temperature and moisture data; *Sci. China Ser. D Earth Sci.* **51** 721–729, https://doi.org/10.1007/s11430-008-0036-1.

Yaseef N R, Yakir D, Rotenberg E, Schiller G and Cohen S 2010 Ecohydrology of a semi-arid forest: Partitioning among water balance components and its implications for predicted precipitation changes; *Ecohydrology* **3** 143–154, https://doi.org/10.1002/eco.65.

Corresponding editor: Kavirajan Rajendran